

Behavior of solitary waves of coupled nonlinear Schrödinger equations subjected to complex external periodic potentials with anti- \mathcal{PT} symmetry

Efstathios G. Charalampidis¹, Fred Cooper^{2,3}, John F. Dawson⁴, Avinash Khare⁵, Avadh Saxena³

¹Department of Mathematics, California Polytechnic State University, San Luis Obispo, CA 93407-0403, United States of America

²The Santa Fe Institute, 1399 Hyde Park Road, Santa Fe, NM 87501, United States of America

³Theoretical Division, Los Alamos National Laboratory, Los Alamos, NM 87545, United States of America

⁴Department of Physics, University of New Hampshire, Durham, NH 03824, United States of America

⁵Physics Department, Savitribai Phule Pune University, Pune 411007, India

E-mail: echarala@calpoly.edu

E-mail: cooper@santafe.edu

E-mail: john.dawson@unh.edu

E-mail: khare@physics.unipune.ac.in

E-mail: avadh@lanl.gov

September 10, 2020 12:31am +00:00

Abstract. We discuss the response of both moving and trapped solitary wave solutions of a nonlinear two-component nonlinear Schrödinger system in 1+1 dimensions to an anti- \mathcal{PT} external periodic complex potential. The dynamical behavior of perturbed solitary waves is explored by conducting numerical simulations of the nonlinear system and using a collective coordinate variational approximation. We present case examples corresponding to choices of the parameters and initial conditions involved therein. The results of the collective coordinate approximation are compared against numerical simulations where we observe qualitatively good agreement between the two. Unlike the case for a single-component solitary wave in a complex periodic \mathcal{PT} -symmetric potential, the collective coordinate equations do not have a small oscillation regime, and initially the height of the two components changes in opposite directions often causing instability. We find that the dynamic stability criteria we have used in the one-component case is proven to be a good indicator for the onset of dynamic instabilities in the present setup.

Keywords: Collective coordinates, variational approach, dissipation functional, spatio-temporal dynamics.

1. Introduction

The study of solitons in nonlinear partial differential equations (PDEs) with non-Hermitian potentials is an important and growing area of research. Specifically, such parity-time or \mathcal{PT} -symmetric PDEs have been studied in detail [1]. Subsequent to the introduction of \mathcal{PT} -symmetry [2] and the ensuing intense research on this topic for a decade and half, the concept of anti- \mathcal{PT} symmetry was first introduced in the context of optics [3] by appropriately arranging the effective optical potential spatially. For anti- \mathcal{PT} -symmetric systems, one has the \mathcal{PT} operator commuting with the Hamiltonian $[H, \mathcal{PT}] = 0$, but in addition $(\mathcal{PT})^2 = -1$ in contrast with the $+1$ as for the \mathcal{PT} -symmetric systems. Its implementation requires the introduction of at least two components in the wave function. Recently, there have been several realizations of the anti- \mathcal{PT} symmetry such as in coupled atom beams [4], optical waveguides with imaginary couplings [5], electrical circuit resonators [6], as well as cold atom based optical four-wave mixing [7]. Moreover, besides optical systems with constant refraction [8], many other experiments have realized the anti- \mathcal{PT} symmetry in atomic [9, 10] and optical [11, 12, 13] systems. In addition, there are several other applications that are related to waveguide arrays [13], spin chains [14], phase transitions [15], diffusive systems [16], information flow [17] as well as non-Markovian processes [18].

Recently, anti- \mathcal{PT} symmetric couplers have been analyzed by Konotop and Zezyulin [19] which lead to lasing and coherent perfect absorption. These systems are experimentally reproduced by having two waveguides locally coupled through an anti- \mathcal{PT} symmetric medium. Here we generalize the treatment of Konotop and Zezyulin to the case of coupled nonlinear Schrödinger equations (NLSEs) which are individually subjected to external potentials as well as coupled by an antisymmetric medium. Such systems can be produced in nonlinear optics in the wave-guiding approximation.

In order to implement anti- \mathcal{PT} symmetry in the NLSE one requires at least a two-component NLSE. Previously we studied exact trapped solitary wave solutions of the two-component NLSE in an external complex supersymmetric potential which had \mathcal{PT} symmetry [20]. In that situation we found regions of stability and instability predicted by both the small oscillation equations for the collective coordinates (CCs), as well as the dynamic criteria and a systematic numerical stability analysis. Although we were able to find exact solutions of the two-component NLSE in some external complex supersymmetric potentials similar to those considered in [20] but having anti- \mathcal{PT} symmetry, all the solutions we have found so far are unstable. To better understand the behavior and stability of solitons in the two-component NLSE in complex external potentials having anti- \mathcal{PT} symmetry, we will study here the simpler question of what happens to stable solitary wave solution of the two-component NLSE when then subjected to an external complex periodic potential having anti- \mathcal{PT} symmetry. This generalizes a previous problem in [21] that we studied for the single-component NLSE solitary wave which was placed in a complex periodic external potential with \mathcal{PT} symmetry.

In the present work, the NLSE soliton solution is a solution of a two-component NLSE. These two-component solitons (individually identified as ψ_1 and ψ_2 hereafter) have the property that they have anti- \mathcal{PT} symmetry, which itself requires that $\psi_2(x, t) = \kappa i \psi_1(-x, -t)$ with $\kappa = \pm 1$. Also for \mathcal{PT} symmetry, the single-component complex external potential we chose previously was of the form $V(x) = a_1 \cos k_1 x + i a_2 \sin k_2 x$. For anti- \mathcal{PT} symmetry, the complex matrix potential, $U(x)$ takes the form $U(x) = \sigma_0 V_0(x) + i \sigma_3 V_1(x) + i \sigma_1 W(x)$, where $V_0 = a_1 \cos k_1 x$, $V_1(x) = a_2 \cos k_2 x$, $W(x) = a_3 \cos k_3 x$, with σ_0 the 2×2 identity matrix, and σ_1 and σ_3 being the Pauli matrices. The second term in the potential changes two things qualitatively. Firstly, calling the initial position of the center of the soliton q_0 , we have that $V_1(x)$ has a minimum at $k_2 q_0 = 0$ and a maximum at $k_2 q_0 = \pi$ with magnitude a_2 . We will show that this prevents us from obtaining a small oscillation expansion for the CC approximation. Related to this, the effect of the σ_3 term in the potential is to cause ψ_1 and ψ_2 to initially grow and decay linearly in time, respectively (or vice versa depending on q_0). This is the main reason for the fact that when $a_2 \neq 0$, the soliton becomes dynamically unstable whether it is trapped or moving. In spite of this, when the soliton experiences the external potential, the widths of both components remain almost identical. This is true also for the position and momentum of each component. The complex potential $i \sigma_1 a_3 \cos k_3 x$ connects directly the two components of the wave function. Having a_3 small and nonzero has minimal effect on changing the “mass” M_i of the two components if a_2 is zero. (Here we define $M_i := \int \psi_i^* \psi_i dx$ for each component.) We show that a CC description of the two-component wave function describes reasonably well the response of the solitary wave to this anti- \mathcal{PT} external potential if we allow the masses and phases of the two components to differ, but keep the position, momentum, width and “chirp” to be the same for both components.

In particular, when $a_3 = 0$, we chose the strength of the two external potentials to match those we used in our single-component case [21]. We also investigated the ability of the dynamical indicator of instability, i.e., whether $dp(t)/dv(t)$ becomes negative [22], to indicate dynamical instability for this two-component NLSE system. Here $q(t)$ and $v(t)$ are canonical variables with $v(t) = \dot{q}(t)$, and $p(t)$ is related to the average value of the momentum operator $-i\partial_x$. This indicator visually shows the instability near where $p(t)$ is turning around from a maximum or a minimum. Since $\sigma_3 V_1(x)$ initially places the two components in opposite directions, it is the major cause for all the various ways that the initial solitary wave can go unstable. These phenomena are reasonably well captured by the eight collective coordinate (8CC) approximation which is compared with direct numerical simulations.

The structure of this paper is as follows. In section 2 we discuss the conditions that anti- \mathcal{PT} symmetry places on the wave function and the external potential. In section 3 we obtain exact moving anti- \mathcal{PT} symmetric solutions of the two-component NLSE and use Derrick’s theorem to show that they are stable to scale transformations. In section 4 we review the CC formalism and in section 5 we introduce our choice of 8CCs, partially motivated by the numerical simulations. In section 6 we show how to

compare the results of the numerical simulation with the time evolution of the CC by relating the CCs to low order moments of the numerically determined wave function. In section 7 we give some typical behaviors for different values of the parameters describing the complex external potential. In section 8 we discuss the stability criterion $dp/dv < 0$ and show that in all the cases we study both the 8CC and numerical determinations of $p(v)$, it leads to the conclusion that these solitary waves are dynamically unstable. In section 9 we state our conclusions and present directions for future study.

2. Anti- \mathcal{PT} systems

In the present work, we consider a two-component nonlinear Schrödinger equation (NLSE) in 1+1 dimensions:

$$\{ i \partial_t + \partial_x^2 + g [\Psi^\dagger(x, t) \Psi(x, t)] - U(x) \} \Psi(x, t) = 0, \quad (2.1)$$

where

$$\Psi(x, t) = \begin{pmatrix} \psi_1(x, t) \\ \psi_2(x, t) \end{pmatrix} \in \mathbb{C}^2 \quad (2.2)$$

is the wave function and g the nonlinearity strength. Here x and t stand for the spatial and temporal variables, respectively, and subscripts in Eq. (2.1) for differentiation with respect to the variables highlighted therein (unless stated otherwise). The matrix function $U(x)$ is the external potential that we describe next.

For two-component systems, the space (\mathcal{P}) and time (\mathcal{T}) reversal operators are defined by:

$$\mathcal{P} \Psi(x, t) = \Psi(-x, t), \quad (2.3a)$$

$$\mathcal{T} \Psi(x, t) = i \sigma_2 \mathcal{K} \Psi(x, -t) \quad (2.3b)$$

$$= \begin{pmatrix} 0 & \mathcal{K} \\ -\mathcal{K} & 0 \end{pmatrix} \begin{pmatrix} \psi_1(x, -t) \\ \psi_2(x, -t) \end{pmatrix} = \begin{pmatrix} \psi_2^*(x, -t) \\ -\psi_1^*(x, -t) \end{pmatrix},$$

where \mathcal{K} is the complex conjugate operator with the property $\mathcal{K}^2 = 1$. The parity and time-reversal operations commute, i.e., $[\mathcal{P}, \mathcal{T}] = 0$, and obey the relations $\mathcal{P}^2 = 1$ and $\mathcal{T}^2 = -1$, so that $(\mathcal{PT})^2 = -1$. Then the \mathcal{PT} operation on Ψ is given by

$$\mathcal{PT} \Psi(x, t) = \begin{pmatrix} \psi_2^*(-x, -t) \\ -\psi_1^*(-x, -t) \end{pmatrix}. \quad (2.4)$$

For anti- \mathcal{PT} symmetry, the linear part of Eq. (2.1) must commute with the \mathcal{PT} operator

$$[\mathcal{PT}, U(x)] = 0 \quad \Rightarrow \quad U(x) = \mathcal{PT} U(x) (\mathcal{PT})^{-1}. \quad (2.5)$$

Let

$$U(x) = \begin{pmatrix} U_0(x) & V_2(x) \\ V_2(x) & U_1(x) \end{pmatrix} \in \mathbb{C}^{2 \times 2}, \quad (2.6)$$

be dependent on x only. Then, (2.5) requires that

$$\begin{aligned} \begin{pmatrix} U_0(x) & V_2(x) \\ V_2(x) & U_1(x) \end{pmatrix} &= \begin{pmatrix} 0 & \mathcal{K} \\ -\mathcal{K} & 0 \end{pmatrix} \begin{pmatrix} U_0(-x) & V_2(-x) \\ V_2(-x) & U_1(-x) \end{pmatrix} \begin{pmatrix} 0 & -\mathcal{K} \\ \mathcal{K} & 0 \end{pmatrix} \\ &= \begin{pmatrix} \mathcal{K}U_1(-x)\mathcal{K} & -\mathcal{K}V_2(-x)\mathcal{K} \\ -\mathcal{K}V_2(-x)\mathcal{K} & \mathcal{K}U_0(-x)\mathcal{K} \end{pmatrix}, \end{aligned} \quad (2.7)$$

from which we conclude that

$$U_0(x) = U_1^*(-x), \quad V_2(x) = -V_2^*(-x). \quad (2.8)$$

Setting $U_0(x) = V_0(x) + iV_1(x)$ with $V_0(x), V_1(x) \in \mathbb{R}$, we find that $U_1(x) = U_0^*(-x) = V_0(-x) - iV_1(-x)$. This way, we can write Eq. (2.6) as

$$U(x) = \begin{pmatrix} V_0(x) + iV_1(x) & V_2(x) \\ V_2(x) & V_0(-x) - iV_1(-x) \end{pmatrix}. \quad (2.9)$$

If we additionally require that $V_0(-x) = V_0(x)$ and $V_1(-x) = V_1(x)$, i.e., V_0, V_1 are even functions, and $V_2(x) := iW(x)$ with $W(x) \in \mathbb{R}$ and even, then $U(x)$ is now given by

$$U(x) = \begin{pmatrix} V(x) & iW(x) \\ iW(x) & V^*(x) \end{pmatrix}, \quad V(x) := V_0(x) + iV_1(x). \quad (2.10)$$

It will be useful to split $U(x)$ into real and imaginary parts via $U(x) := U_0(x) + iU_1(x)$, where

$$U_0(x) = \begin{pmatrix} V_0(x) & 0 \\ 0 & V_0(x) \end{pmatrix}, \quad U_1(x) = \begin{pmatrix} V_1(x) & W(x) \\ W(x) & -V_1(x) \end{pmatrix}. \quad (2.11)$$

Calling $\sigma_0 = \mathbb{I}_2$, i.e., the 2×2 unit matrix, we can write

$$U(x) = \sigma_0 V_0(x) + i\sigma_3 V_1(x) + i\sigma_1 W(x). \quad (2.12)$$

Eigenstates of the anti- \mathcal{PT} operator satisfy the equation

$$\mathcal{PT} \Psi_\kappa(x, t) = \kappa i \Psi_\kappa(x, t), \quad \kappa = \pm 1, \quad (2.13)$$

from which we conclude that the components satisfy:

$$\psi_{2\kappa}(x, t) = \kappa i \psi_{1\kappa}^*(-x, -t). \quad (2.14)$$

3. Exact solitary wave solutions when $U(x) \equiv 0$

In the absence of external potentials, Eq. (2.1) reduces to:

$$\{i\partial_t + \partial_x^2 + g(|\psi_1(x, t)|^2 + |\psi_2(x, t)|^2)\} \psi_1(x, t) = 0, \quad (3.1a)$$

$$\{i\partial_t + \partial_x^2 + g(|\psi_1(x, t)|^2 + |\psi_2(x, t)|^2)\} \psi_2(x, t) = 0, \quad (3.1b)$$

whence it is easy to show that the traveling solitary wave solution

$$\psi_1(x, t) = A_1 \beta \operatorname{sech}[\beta(x - vt)] \exp\{i[p(x - vt) - \theta(t)]\}, \quad (3.2a)$$

$$\psi_2(x, t) = A_2 \beta \operatorname{sech}[\beta(x - vt)] \exp\{i[p(x - vt) - \theta(t)]\}, \quad (3.2b)$$

with real frequencies is an exact solution of (3.1a) provided that

$$g(|A_1|^2 + |A_2|^2) = 2, \quad p = \frac{v}{2}, \quad \theta(t) = -(p^2 + \beta^2)t. \quad (3.3)$$

These solutions are eigenstates of the anti- \mathcal{PT} operator $\forall x, t$ if

$$A_2 = i \kappa A_1^*, \quad \kappa = \pm 1, \quad (3.4)$$

in which case, if we set $A_1 = A$ and $A_2 = i \kappa A$, then $A^2 = 1/g$. Normalization integrals are given by:

$$M_1 = \int dx |\psi_1(x, t)|^2 = 2\beta A_1^2, \quad M_2 = \int dx |\psi_2(x, t)|^2 = 2\beta A_2^2, \quad (3.5)$$

such that the condition in Eq. (3.3) becomes $g(M_1 + M_2) = 4\beta$. Given now this form of the exact solution, the self-interaction potential term commutes with the \mathcal{PT} operator $\forall t$. For the soliton at rest, Eq. (3.2a) reduces to

$$\psi_1(x, t) = A \beta \operatorname{sech}(\beta x) \exp\{i(-\beta^2 t)\}, \quad (3.6a)$$

$$\psi_2(x, t) = A \beta \operatorname{sech}(\beta x) \exp\{i(-\beta^2 t \pm \pi/2)\}. \quad (3.6b)$$

3.1. Derrick's theorem

We can use the scaling argument of Derrick [23] to determine if the two-component static solutions of (3.6a) are stable to scale transformations. For the sake of completeness in the present discussion, we introduce the nonlinearity exponent, identified as k hereafter, which allows us to show that the stability depends on k . For the single-component NLSE at hand, the solutions are unstable to either blowup or collapse when $k > 2$ [24]. Here we will confirm that the exact solutions we found for $k = 1$ are stable to scale transformations. To that effect, let us recall first the Hamiltonian given itself by

$$H = \int dx \left\{ \frac{1}{2} |\partial_x \Psi(x)|^2 - \frac{g}{k+1} [\Psi^\dagger(x)\Psi(x)]^{k+1} \right\}, \quad (3.7)$$

where $\Psi(x)$ denotes the static two-component solution of (3.1a). It is well known that using stability with respect to scale transformation to understand domains of stability applies to this type of Hamiltonian. If we make the scale transformation of the solution of the form

$$\Psi(x) \mapsto \alpha^{1/2} \Psi(\alpha x) = \alpha^{1/2} \Psi(y), \quad y := \alpha x \quad (3.8)$$

which preserves the normalization, i.e., $M = \int dx |\Psi(x)|^2$, we obtain

$$H = \alpha^2 H_1 - \alpha^k H_2, \quad (3.9)$$

where

$$H_1 = \frac{1}{2} \int dy |\partial_y \Psi(y)|^2 > 0, \quad (3.10)$$

$$H_2 = \frac{g}{k+1} \int dy [\Psi^\dagger(y)\Psi(y)]^{k+1} > 0, \quad (3.11)$$

for all k as well as

$$\frac{\partial H(\alpha)}{\partial \alpha} = 2\alpha H_1 - k \alpha^{k-1} H_2, \quad (3.12a)$$

$$\frac{\partial^2 H(\alpha)}{\partial \alpha^2} = 2 H_1 - k(k-1) \alpha^{k-2} H_2. \quad (3.12b)$$

Setting the first (partial) derivative to zero at $\alpha = 1$ gives an equation consistent with the equations of motion:

$$kH_2 = 2H_1, \quad (3.13)$$

whereas the second derivative evaluated at the minimum, and at $\alpha = 1$ reads

$$\left. \frac{\partial^2 H(\alpha)}{\partial \alpha^2} \right|_{\alpha=1} = k(2-k)H_2. \quad (3.14)$$

Thus, we see that at $k = 1$, the exact solutions for the free case are stable. Only when $k > 2$ do the solutions become unstable to scale transformations. However, once one adds the external complex potential terms, the windows of stability need to be determined by the stability curve $p(v)$ or by simulations of the NLSE equation.

It should be noted in passing that for $k = 1$ and using Eq. (3.6a), we have that

$$H_1 = (M_1 + M_2)\beta^2/3, \quad (3.15a)$$

$$H_2 = g(M_1 + M_2)^2\beta/6, \quad (3.15b)$$

so that imposing (3.13) for $k = 1$ gives $g(M_1 + M_2) = 4\beta$. This is satisfied by the exact solution.

4. Collective coordinates

We consider in this work external potentials of the form:

$$V_0(x) = a_1 \cos k_1 x, \quad (4.1a)$$

$$V_1(x) = a_2 \cos k_2 x, \quad (4.1b)$$

$$W(x) = a_3 \cos k_3 x, \quad (4.1c)$$

which are (all real and) even functions of x . For $V_0(x)$ to be confining near $x = 0$ we need $a_1 < 0$. We review here the method of CCs (see for example Ref. [25]) applied to our case. The time-dependent variational approximation relies on introducing a finite set of time-dependent real parameters in a trial wave function that hopefully captures the time evolution of a perturbed solution. By doing this, one obtains a simplified set of ordinary differential equations (ODEs) for the CCs in place of solving the full PDE for the NLS equation. To this end, let us first set

$$\begin{aligned} \Psi(x, t) &\mapsto \Psi[x, Q(t)] \\ Q(t) &= \{ Q^1(t), Q^2(t), \dots, Q^{2n}(t) \} \in \mathbb{R}^{2n}, \end{aligned} \quad (4.2)$$

where $Q(t)$ are the CCs. We note that the success of the method depends greatly on the choice of the trial wave function $\tilde{\Psi}[x, Q(t)]$. The generalized dissipative Euler-Lagrange equations lead to Hamilton's equations for $Q(t)$. The Lagrangian in terms of $Q(t)$ is given by

$$L(Q, \dot{Q}) = T(Q, \dot{Q}) - H(Q) \quad (4.3)$$

with the dynamic term

$$\begin{aligned} T(Q, \dot{Q}) &= \frac{i}{2} \int dx \{ \Psi^\dagger(x, Q) \Psi_t(x, Q) - \Psi_t^\dagger(x, Q) \Psi(x, Q) \} \\ &= \pi_\mu(Q) \dot{Q}^\mu, \end{aligned} \quad (4.4)$$

and $\pi_{\mu(Q)}$ defined via

$$\pi_\mu(Q) = \frac{i}{2} \int dx \{ \Psi^\dagger(x, Q) [\partial_\mu \Psi(x, Q)] - [\partial_\mu \Psi^\dagger(x, Q)] \Psi(x, Q) \}, \quad (4.5)$$

where $\partial_\mu := \partial/\partial Q^\mu$. The Hamiltonian $H(Q)$ is given by

$$H(Q) = \int dx \left\{ |\partial_x \Psi(x, Q)|^2 - \Psi^\dagger(x, Q) U_0(x) \Psi(x, Q) - \frac{g}{2} |\Psi(x, Q)|^4 \right\}, \quad (4.6)$$

and on an equal footing, the dissipation functional (again, in terms of the CCs) is respectively given by

$$\begin{aligned} F(Q, \dot{Q}) &= i \int dx \{ \Psi^\dagger(x, Q) U_1(x) \Psi_t(x, Q) - \Psi_t^\dagger(x, Q) U_1(x) \Psi(x, Q) \} \\ &= w_\mu(Q) \dot{Q}^\mu, \end{aligned} \quad (4.7)$$

where

$$w_\mu(Q) = i \int dx \{ \Psi^\dagger(x, Q) U_1(x) [\partial_\mu \Psi(x, Q)] - [\partial_\mu \Psi_t^\dagger(x, Q) U_1(x) \Psi(x, Q)] \} \quad (4.8)$$

with $U_0(x)$ and $U_1(x)$ being given by Eq. (2.11).

This way, the generalized Euler-Lagrange equations read

$$\frac{\partial L}{\partial Q^\mu} - \frac{d}{dt} \left(\frac{\partial L}{\partial \dot{Q}^\mu} \right) = - \frac{\partial F}{\partial \dot{Q}^\mu}. \quad (4.9)$$

If $v_\mu(Q) := \partial_\mu H(Q)$, we find

$$f_{\mu\nu}(Q) \dot{Q}^\nu = u_\mu(Q) = v_\mu(Q) - w_\mu(Q), \quad (4.10)$$

where

$$f_{\mu\nu}(Q) = \partial_\mu \pi_\nu(Q) - \partial_\nu \pi_\mu(Q) \quad (4.11)$$

is an antisymmetric $2n \times 2n$ symplectic matrix. If $\det(f(Q)) \neq 0$, we can define an inverse as the contra-variant matrix with upper indices,

$$f^{\mu\nu}(Q) f_{\nu\sigma}(Q) = \delta_\sigma^\mu, \quad (4.12)$$

in which case the equations of motion (4.10) can be put in the symplectic form:

$$\dot{Q}^\mu = f^{\mu\nu}(Q) u_\nu(Q). \quad (4.13)$$

5. Eight parameter time-dependent collective coordinates

From Eqs. (2.1) and (2.10), the coupled equations we wish to solve are given by

$$\{i\partial_t + \partial_x^2 - V(x) + g(|\psi_1(x,t)|^2 + |\psi_2(x,t)|^2)\} \psi_1(x,t) - iW(x)\psi_2(x,t) = 0, \quad (5.1a)$$

$$\{i\partial_t + \partial_x^2 - V^*(x) + g(|\psi_1(x,t)|^2 + |\psi_2(x,t)|^2)\} \psi_2(x,t) - iW(x)\psi_1(x,t) = 0. \quad (5.1b)$$

We choose time-dependent variational wave functions of the form:

$$\psi_1[x, Q(t)] = A_1(t) \beta(t) \operatorname{sech}[\beta(t)(x - q(t))] e^{i[\phi[x, Q(t)] - \theta_1(t)]}, \quad (5.2a)$$

$$\psi_2[x, Q(t)] = A_2(t) \beta(t) \operatorname{sech}[\beta(t)(x - q(t))] e^{i[\phi[x, Q(t)] - \theta_2(t)]}, \quad (5.2b)$$

where

$$\phi[x, Q(t)] = p(t)(x - q(t)) + \Lambda(t)(x - q(t))^2. \quad (5.3)$$

For the variational solutions, we define

$$M_1(t) =: \int dx |\psi_1[x, Q(t)]|^2 = 2\beta(t) |A_1(t)|^2, \quad (5.4a)$$

$$M_2(t) =: \int dx |\psi_2[x, Q(t)]|^2 = 2\beta(t) |A_2(t)|^2. \quad (5.4b)$$

We will choose as our CCs the set of eight quantities:

$$Q = \{M_1, \theta_1, M_2, \theta_2, q, p, \beta, \Lambda\}, \quad (5.5)$$

with the canonical pairs,

$$\{M_1(t), \theta_1(t)\}, \quad \{M_2(t), \theta_2(t)\}, \quad \{q(t), p(t)\}, \quad \{\beta(t), \Lambda(t)\}. \quad (5.6)$$

The CCs $Q(t)$ are related to the low order moments of the coordinate and momentum operators so that their actual behavior can be determined from the numerical simulation of the NLSE. This choice of CCs was determined after the numerical simulations suggested that the widths, position, and momenta of the two components followed one another closely (even though they were not exactly equal as we will see in our numerical simulations).

5.1. Initial conditions

At $t = 0$, we require that the variational wave functions [cf. Eqs. (5.2a)] match the traveling wave solution of Eq. (3.2a) with no external potential. In addition, we require that initially the wave function is an eigenstate of the anti- \mathcal{PT} operator. Furthermore, we choose $g = 2$ and $\beta(0) = 1/2$ in order to draw direct comparisons with our previous work on the NLSE in a \mathcal{PT} -symmetric potential [21]. This means that at $t = 0$ we set

$$\beta(0) = 1/2, \quad \Lambda(0) = 0, \quad \theta_1(0) = 0, \quad \theta_2(0) = \kappa\pi/2, \quad M_1(0) = M_2(0) = 1/2, \quad (5.7)$$

so that $A_1(0) = A_2(0) = 1/\sqrt{2}$. Plots of the potentials and initial variational wave functions are shown in Fig. 1 where we have set $q(0) = \pi$. Note that the magnitudes of the two wave functions are identical at $t = 0$.

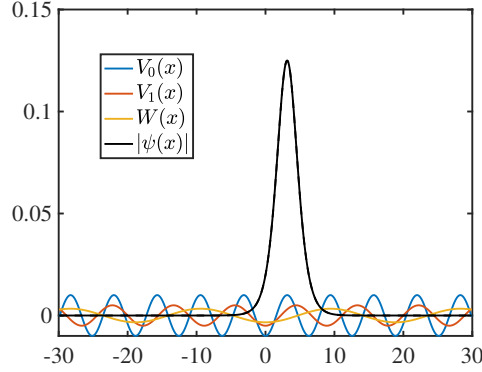


Figure 1. (Color online) Potentials and initial wave functions for 8CC variational calculations for the parameters of Section 5.1 with $q(0) = \pi$. Here we have set $a_1 = -1/100$, $a_2 = -1/200$, and $a_3 = -1/300$ with $k_1 = 1$, $k_2 = 1/\sqrt{2}$, and $k_3 = 1/3$.

5.2. Equations of motion

Following the method described in Section 4, and using the variational wave function (5.2a), we find the following equations of motion for the 8CCs:

$$\dot{M}_1 = a_2 M_1 \cos(k_2 q) G_1(k_2/\beta) \quad (5.8a)$$

$$\begin{aligned} & + a_3 \sqrt{M_1 M_2} \cos(k_3 q) \cos(\theta_1 - \theta_2) G_1(k_3/\beta), \\ \dot{\theta}_1 = & -p^2 + \frac{2}{3} \beta^2 + \frac{a_1}{2} \cos(k_1 q) \left[G_1(k_1/\beta) - \frac{k_1}{2\beta} G_1'(k_1/\beta) \right] - \frac{5}{12} g \beta M \\ & + a_2 \frac{p}{\beta} \frac{M_1 - M_2}{M} \sin(k_2 q) G_3(k_2/\beta) \end{aligned} \quad (5.8b)$$

$$\begin{aligned} & - (a_3/2) \sqrt{M_2/M_1} \cos(k_3 q) \sin(\theta_1 - \theta_2) G_1(k_3/\beta) \\ & + a_3 \sqrt{M_1 M_2/M^2} (2p/\beta) \sin(k_3 q) \cos(\theta_1 - \theta_2) G_3(k_3/\beta), \\ \dot{M}_2 = & -a_2 M_2 \cos(k_2 q) G_1(k_2/\beta) \end{aligned} \quad (5.8c)$$

$$\begin{aligned} & + a_3 \sqrt{M_1 M_2} \cos(k_3 q) \cos(\theta_1 - \theta_2) G_1(k_3/\beta), \\ \dot{\theta}_2 = & -p^2 + \frac{2}{3} \beta^2 + \frac{a_1}{2} \cos(k_1 q) \left[G_1(k_1/\beta) - \frac{k_1}{2\beta} G_1'(k_1/\beta) \right] - \frac{5}{12} g \beta M \\ & + a_2 \frac{p}{\beta} \frac{M_1 - M_2}{M} \sin(k_2 q) G_3(k_2/\beta) \end{aligned} \quad (5.8d)$$

$$\begin{aligned} & - (a_3/2) \sqrt{M_1/M_2} \cos(k_3 q) \sin(\theta_1 - \theta_2) G_1(k_3/\beta) \\ & + a_3 \sqrt{M_1 M_2/M^2} (2p/\beta) \sin(k_3 q) \cos(\theta_1 - \theta_2) G_3(k_3/\beta), \\ \dot{q} = & 2p - \frac{a_2}{\beta} \frac{M_1 - M_2}{M} \sin(k_2 q) G_3(k_2/\beta) \end{aligned} \quad (5.8e)$$

$$\begin{aligned} & - a_3 \sqrt{M_1 M_2/M^2} \sin(k_3 q) \cos(\theta_1 - \theta_2) (2/\beta) G_3(k_3/\beta), \\ \dot{p} = & \frac{k_1 a_1}{2} \sin(k_1 q) G_1(k_1/\beta) - a_2 \frac{M_1 - M_2}{M} \frac{2\Lambda}{\beta} \sin(k_2 q) G_3(k_2/\beta) \\ & - a_3 (4\Lambda/\beta) \sqrt{M_1 M_2/M^2} \sin(k_3 q) \cos(\theta_1 - \theta_2) G_3(k_3/\beta), \end{aligned} \quad (5.8f)$$

$$\dot{\beta} = -4\beta\Lambda + \frac{M_1 - M_2}{M} a_2 \cos(k_2 q) \frac{\beta}{2} [G_1(k_2/\beta) - (12/\pi^2) G_2(k_2/\beta)] \quad (5.8g)$$

$$+ a_3 \beta \sqrt{M_1 M_2 / M^2} \cos(k_3 q) \cos(\theta_1 - \theta_2) [G_1(k_3/\beta) - (12/\pi^2) G_2(k_3/\beta)],$$

$$\dot{\Lambda} = -4\Lambda^2 + \frac{4\beta^4}{\pi^2} + a_1 \frac{6k_1\beta}{\pi^2} G_1'(k_1/\beta) - \frac{g\beta^3}{\pi^2} M. \quad (5.8h)$$

Details of this derivation are given in Appendix A.

5.3. General Observations about the 8CC equations

Firstly, we note that M_1 and M_2 go in opposite directions from their initial yet equal value due to $a_2 \neq 0$. This often leads to one of the two masses going to zero. We further note that when $a_2 = 0$, the effect of a_3 on the dynamics is proportional to $\cos(\theta_1 - \theta_2)$ which initially is zero. Moreover, $M_1(0) = M_2(0)$ due to anti- \mathcal{PT} initial conditions. The equation for $\dot{\theta}_1 - \dot{\theta}_2$ is given by

$$\dot{\theta}_1 - \dot{\theta}_2 = \frac{\pi a_3}{2\beta} \left[\left(\sqrt{\frac{M_2}{M_1}} - \sqrt{\frac{M_1}{M_2}} \right) \cos(q(t)/4) \operatorname{csch}(\pi/(8\beta)) \sin(\theta_1 - \theta_2) \right]. \quad (5.9)$$

Since the derivative is initially zero because the two masses are the same (unless M_1 differs greatly from M_2), $\theta_1 - \theta_2$ stays small, and the presence of a_3 does not change the CC equations for q, p, β, M_1, M_2 greatly from the case when $a_3 = 0$.

5.4. Small oscillation equations when $a_2 = a_3 = 0$

When $a_2 < 0$, M_1 and M_2 initially decrease and increase with time, respectively (or vice versa depending on the sign of $\cos k_2 x_0$), so one is never in the small oscillation regime. However when $a_2 = a_3 = 0$ small oscillations are possible in the potential $V_0(x)$. In the small deviation from the static soliton regime, the update equations for the set (q, p) decouple from the set (β, Λ) . The relevant equations when $a_2 = a_3 = 0$ are

$$\dot{q} = 2p, \quad \dot{p} = \frac{k_1 a_1}{2} \sin(k_1 q) G_1(k_1/\beta), \quad (5.10)$$

$$\dot{\beta} = -4\beta\Lambda, \quad \dot{\Lambda} = -4\Lambda^2 + \frac{4\beta^4}{\pi^2} + a_1 \frac{6k_1\beta}{\pi^2} G_1'(k_1/\beta) - \frac{g\beta^3}{\pi^2} M.$$

Setting $\beta(t) = 1/2 + \delta\beta(t)$ with $\delta\beta(t) \ll 1 \forall t$ (and all the other parameters assumed small deviations from zero), one has for the first two equations in (5.10):

$$\dot{q}(t) = 2p(t), \quad \dot{p}(t) = [a_1 k_1^3 \pi \operatorname{csch}(k_1 \pi)] q(t). \quad (5.11)$$

Since $a_1 < 0$, we have that the frequency of both p and q (in this small oscillation regime) is just

$$\omega_q^2 = 2|a_1| k_1^3 \pi \operatorname{csch}(k_1 \pi). \quad (5.12)$$

For instance, if $a_1 = -1/100$ and $k_1 = 1$, the period T_q is given by

$$T_q = \frac{2\pi}{\omega_q} = \sqrt{\frac{2\pi}{a_1 k_1^3 \operatorname{csch}(\pi k_1)}} \approx 85.2. \quad (5.13)$$

Since initially $gM = 4\beta(0) = 2$, we find (ignoring the a_1 correction)

$$\delta\dot{\beta} = -2\delta\Lambda, \quad \delta\dot{\Lambda} = \frac{\delta\beta}{2\pi^2}, \quad (5.14)$$

such that

$$\omega_\beta = \frac{1}{\pi}, \quad T_\beta = \frac{2\pi}{\omega_\beta} = 2\pi^2 \approx 19.7392. \quad (5.15)$$

To include the a_1 correction, one can use

$$G'_1(k_1/\beta) \rightarrow 2\pi^2 k_1 \delta\beta [\pi k_1 - 2\pi k_1 \coth^2(\pi k_1) + 2 \coth(\pi k_1)] \operatorname{csch}(\pi k_1) \\ + \pi [1 - \pi k_1 \coth(\pi k_1)] \operatorname{csch}(\pi k_1). \quad (5.16)$$

6. Comparison of Numerical Simulations with 8CC equations evolution

In solving for the time evolution of the NLSE in these external potentials, we will employ initial conditions corresponding to the exact solution of the NLSE in the free case. The configuration space of possible solutions (and their associated time evolution) is huge, and we will just exhibit five cases to give the general idea of how well the CC approach matches with the time evolution of the NLSE. We have chosen parameters to be similar to those used in our previous work on the single-component \mathcal{PT} -symmetric NLSE.

The cases we study hereafter are presented in Table 1 and summarize several behaviors we identified. We have chosen q_0 so that as far as V_0 is concerned, the initial wave function is starting at either a minimum of the potential ($q_0 = 0$), or a maximum of the potential ($q_0 = \pi$). In particular, in cases 1 and 5, the soliton is trapped by the potential V_0 . In case 1, all k_i are different and $q_0 = \pi$. In case 5 we have instead $k_i = 1$, $q_0 = 0$. Case 2 is a moving soliton that is unstable. Case 3 shows the effect of a_3 on a moving soliton when $a_2 = 0$. To first-order approximation the result is similar to the case where $a_3 = 0$ in that the width of both components just oscillates, and (at least for a reasonable amount of time) the two components stay equal in mass and these masses do not change in time. Case 4 shows what happens when we add a_2 to case 3, which then causes M_1 to gradually increase, and M_2 to gradually decrease. This situation is unstable as the total mass $M_1 + M_2$ gradually increases. The initial values of the parameters we use for the CC simulations are also given in Table 1. These parameters also determine the initial wave function used in our numerical simulations. The values of q_0 and p_0 were chosen so that a comparison with simulations in the one-component case could be made. If we increase a_2 in magnitude much beyond $|a_2| = 1/300$, then the instabilities manifest themselves at quite earlier times.

The cases shown in Table 1 are explored by performing numerical simulations at the level of Eqs. (5.1a)-(5.1b). At first, the infinite spatial domain is truncated into a finite one $[-L, L]$, and then a one-dimensional spatial grid of equidistant points with resolution Δx is introduced ($L = 30$ and $\Delta x = 0.1$ in this work). The Laplacian in Eqs. (5.1a)-(5.1b) is replaced by a second-order accurate, finite difference scheme. We impose zero Dirichlet boundary conditions at the edges of our computational domain,

Table 1. Parameters for simulations. In all cases we take $g = 2$, $M_1(0) = M_2(0) = 1/2$, $\beta_1(0) = \beta_2(0) = 1/2$, and $\Lambda_1(0) = \Lambda_2(0) = 0$, and with $\theta_1(0) = 0$, $\theta_2(0) = \pi/2$.

Case	a_1	a_2	a_3	k_1	k_2	k_3	$q(0)$	$p(0)$
1	-1/100	-1/500	-1/1000	1	$1/\sqrt{2}$	1/3	π	.001
2	-1/100	-1/100	-1/500	1	1/3	1/4	π	-0.0457
3	-1/100	0	-1/100	1	1	1	π	0.0531649
4	-1/100	-1/1000	-1/100	1	1	1	π	0.0531649
5	-1/100	-1/1000	-1/100	1	1	1	0	0.0531649

that is, $\psi_{1,2}(x = \pm L, t) = 0$, $\forall t \geq 0$. As a result, the coupled NLSEs reduce into a (large) system of ODEs that are advanced forward in time by employing the Dormand and Prince method with time step-size adaptation [28]. When the dynamics revealed an instability of the pertinent waveforms, we stopped the integrator before they hit the boundary. Also, we corroborated our numerical results by considering a fourth-order accurate, finite difference scheme for the Laplacian operator. We found that both discretization schemes produce identical results.

To compare the numerical simulation results of the NLSEs with the 8CC equations we use the fact that we can extract the values of the CCs from the various low order moments of the numerically obtained wave function. In fact, the equations the low order moment equations obey are an alternative way of obtaining equations that are equivalent to those obtained from the variational approach. Assuming a more general variational wave function ansatz where we allow different values for the expectation of xp, x^2, p, px for each component of the wave function, we can extract easily the values of all these time evolving parameters from the moments of the numerical solution. In particular, let us assume that each component of the wave function can be parametrized as

$$\begin{aligned} \psi_i[x, Q(t)] &= A_i(t) \beta_i(t) \operatorname{sech}[\beta_i(t)(x - q_i(t))] e^{i[\phi_i[x, Q(t)] - \theta_i(t)]}, \\ \phi_i[x, Q(t)] &= p_i(t)(x - q_i(t)) + \Lambda_i(t)(x - q_i(t))^2. \end{aligned} \quad (6.1)$$

The n^{th} moment of the density distribution for each component of the wave function is defined by

$$\begin{aligned} \mathcal{M}_n^i(t) &= \int dx x^n |\psi_i(x, t)|^2 \\ &= \frac{M_i(t)}{2} \int dy \left[\frac{y}{\beta_i(t)} + q_i(t) \right]^n \operatorname{sech}^2(y), \end{aligned} \quad (6.2)$$

which gives

$$\mathcal{M}_0^i(t) = M_i(t), \quad (6.3a)$$

$$\mathcal{M}_1^i(t) = M_i(t) q_i(t), \quad (6.3b)$$

$$\mathcal{M}_2^i(t) = M_i(t) \left[q_i^2(t) + \frac{\pi^2}{12} \frac{1}{\beta_i^2(t)} \right]. \quad (6.3c)$$

Note that from Eqs. (6.3a), we can find $M_i(t)$, $q_i(t)$, and $\beta_i(t)$. On an equal footing, the n^{th} moment of the momentum operator is defined by

$$\begin{aligned} \mathcal{P}_n^i(t) &= \frac{1}{2i} \int dx x^n \{ \psi_i^*(x, t) [\partial_x \psi_i(x, t)] - [\partial_x \psi_i^*(x, t)] \psi_i(x, t) \} \\ &= \int dx x^n \text{Im} \{ \psi_i^*(x, t) [\partial_x \psi_i(x, t)] \}, \end{aligned} \quad (6.4)$$

which gives

$$\mathcal{P}_0^i(t) = M_i(t) p_i(t), \quad (6.5a)$$

$$\mathcal{P}_1^i(t) = M_i(t) \left[p_i(t) q_i(t) + \frac{\pi^2 \Lambda_i(t)}{6 \beta_i^2(t)} \right], \quad (6.5b)$$

from which we can find $p_i(t)$ and $\Lambda_i(t)$. Finally, for the phase, we compute:

$$\begin{aligned} \mathcal{E}_0^i(t) &= \frac{i}{2} \int dx \{ \psi_i^*(x, t) [\partial_t \psi_i(x, t)] - [\partial_t \psi_i^*(x, t)] \psi_i(x, t) \} \\ &= M_i(t) \left\{ \left[p_i(t) - \frac{\pi^2}{6} \frac{\Lambda_i(t)}{\beta_i(t)} \right] \dot{q}_i(t) + \dot{\theta}_i(t) \right\}, \end{aligned} \quad (6.6)$$

from which we can find $\dot{\theta}_i(t)$. We expect the time evolution of the higher moments of the coordinate and momentum operators (i.e. β and Λ of our variational ansatz) to become less accurate than the time evolution of the lower moments, which seems to be the case in our simulations. What is remarkable is that to a good approximation, we find that using the moments of the numerical simulations of the wave function, the moments have the property that

$$q_1(t) = q_2(t), \quad p_1(t) = p_2(t), \quad \beta_1(t) = \beta_2(t), \quad \Lambda_1(t) = \Lambda_2(t), \quad (6.7)$$

so one can use a trial wave function with 8 instead of 12 CCs.

7. Discussion of Typical Behaviors

In this section, we show some typical behaviors which are quite dependent on the parameters chosen (see Table 1). If one looks at the potential $V_0(x)$ in Fig. 1, we see it has maxima at $x = \pi$ and $x = 3\pi$ (in general at $x = (2n + 1)\pi/k_1$ with $n \in \mathbb{Z}$) so if the soliton has a small initial momentum in the positive direction it can lead to the behavior seen in Fig. 2. For this case, the soliton stays trapped between $\pi < x < 3\pi$ (see the panel showcasing $q(t)$ therein). At later times ($t > 300$) in the CC evolution one sees a very slight reduction in amplitude of the q oscillations. Note that $\beta(t)$ continues to oscillate about $\beta(t) = 0.47$ and $\Lambda(t)$ about zero. Also, $M_1(t)$ is creeping up linearly with a very small slope, and $M_2(t)$ is decreasing linearly with a small slope such that the time averaged value of $M_1 + M_2$ is remaining near one. However the amplitudes of oscillations of $M_1 + M_2$ have almost reached one percent by $t = 100$. Here $p(v)$ indicates that this case is dynamically unstable as seen in Fig. 7. When we compare the CC results to the numerical simulations, we find that the CCs are much closer to the numerical results for the lower order moments, but even $\beta(t)$ and $\Lambda(t)$ give qualitatively

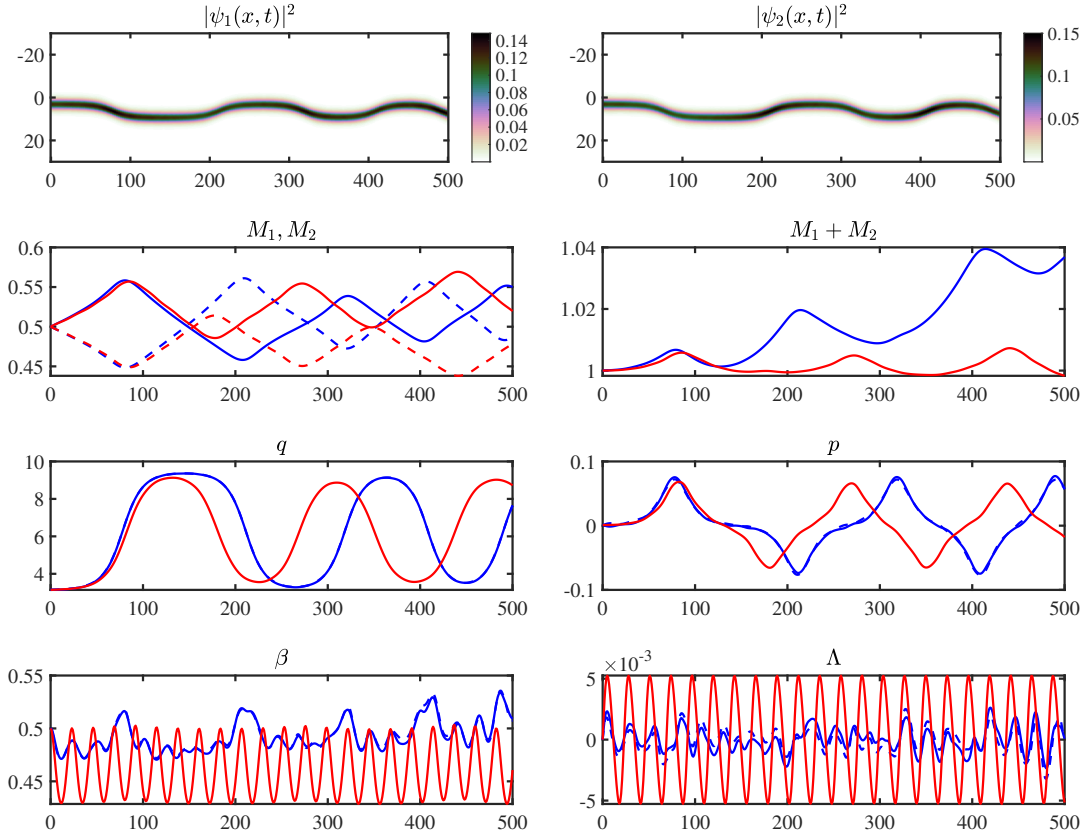


Figure 2. (Color online) Numerical results corresponding to parameters and initial conditions for case 1 of Table 1. The top left and right panels demonstrate the spatio-temporal evolution of the densities $|\psi_1|^2$ and $|\psi_2|^2$, respectively. The blue lines in the second, third, and fourth rows correspond to numerical results of the Schrödinger's equation whereas the red lines to the 8CC variational calculation. The solid and dashed lines correspond to the first and second component, respectively. We see that around $t = 200$ the variational approximation starts diverging quantitatively from the numerical result.

good results. We notice that β and Λ have a secondary oscillation frequency that is not captured by the CC equations. This is typical of what happens when the soliton is trapped by $V_0(x)$.

The second example is shown in Fig. 3 and corresponds to case 2 of Table 1. Here, we chose different periods for the three potentials. This is a moving soliton where now $M_1(t)$ is decreasing slowly in time and $M_2(t)$ increasing in time. Here $\beta(t)$ as well as $M_1 + M_2$ are increasing in time indicating eventual blowup of the solitary wave. The magnitudes of the oscillations of $p(t)$ and $\dot{q}(t)$ are decreasing in time, and at each turnaround $dp/dv < 0$, thus indicating an unstable case. This behavior of $p(v)$ is shown in Fig. 7.

Case 3 is shown in Fig. 4. Here we consider the effect of a_2 on a moving soliton when $k_i = 1$ for $i = 1, 2, 3$. The 8CC approximation in this case gives $M_1 = M_2 = 1/2$ for all time so that the effect of a_2 on the motion in the real potential $V_0(x)$ is minimal.

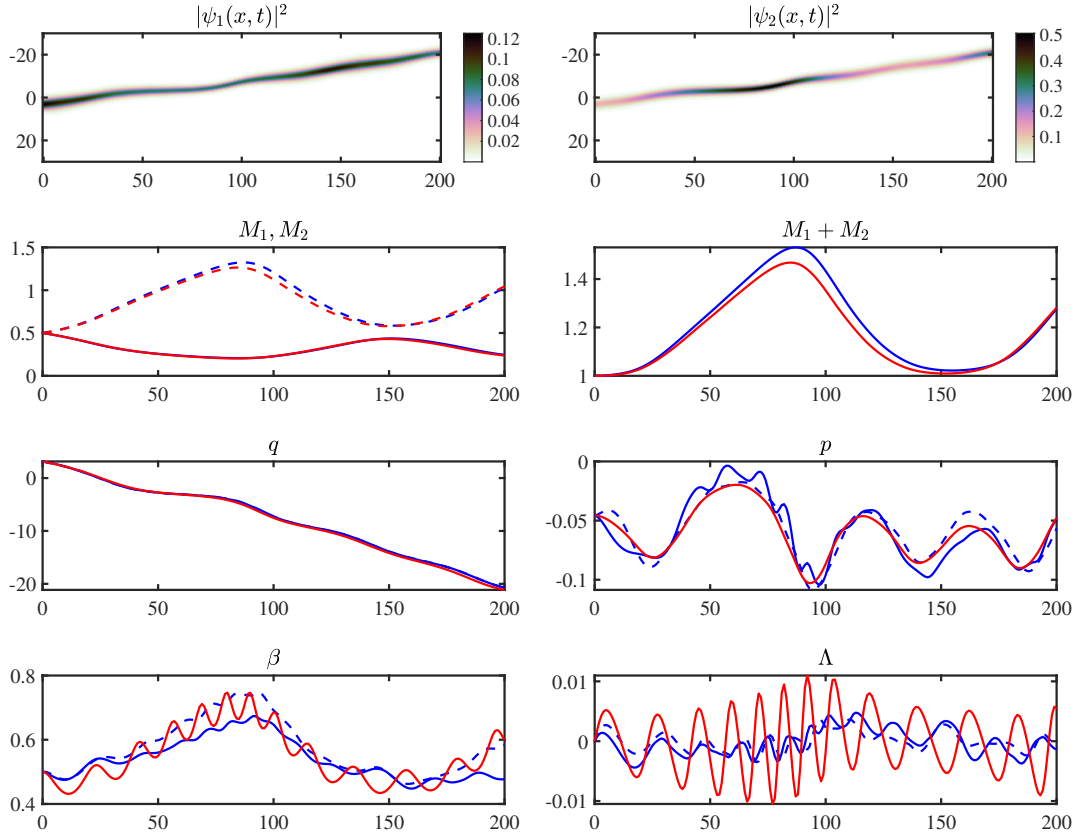


Figure 3. (Color online) Same as Fig. 2 but for the case 2 of Table 1. The top left and right panels demonstrate the spatio-temporal evolution of the densities $|\psi_1|^2$ and $|\psi_2|^2$, respectively. The blue lines in the second, third, and fourth rows correspond to numerical results of the Schrödinger's equation whereas the red lines to the 8CC variational calculation. The solid and dashed lines correspond to the first and second component, respectively.

The actual numerics show that the 8CC approximation is breaking down although the parameters $q(t)$, $p(t)$, $\beta(t)$, and $\Lambda(t)$ are qualitatively the same for both components (in fact, they differ so that the total mass $M_1 + M_2$ very slowly increases).

Case 4 is shown in Fig. 5. Here we have a moving soliton starting at $q_0 = \pi$ and the same initial conditions as in case 3 but we now turn on $a_2 = -1/1000$. This causes M_1 to slowly increase, and M_2 to slowly decrease, with $M_1 + M_2$ slowly increasing which eventually leads to blowup. This instability is seen in the $p(v)$ curve shown in 7. Here we start seeing a divergence from the solid blue lines for $q(t)$, $p(t)$, $\beta(t)$, and $\Lambda(t)$ from the dashed blue lines in the numerical simulations, indicating a slight breakdown in our assumption that the two components have the same values. Nevertheless the 8CC parameters follow reasonably well the numerically obtained moments.

Case 5 is shown in Fig. 6. Here we have a moving soliton starting at $q_0 = 0$ but otherwise the same initial conditions as case 4. This results in the soliton being trapped in the well of $V_0(x)$. Here M_1 slowly decreases and M_2 slowly increases, opposite to

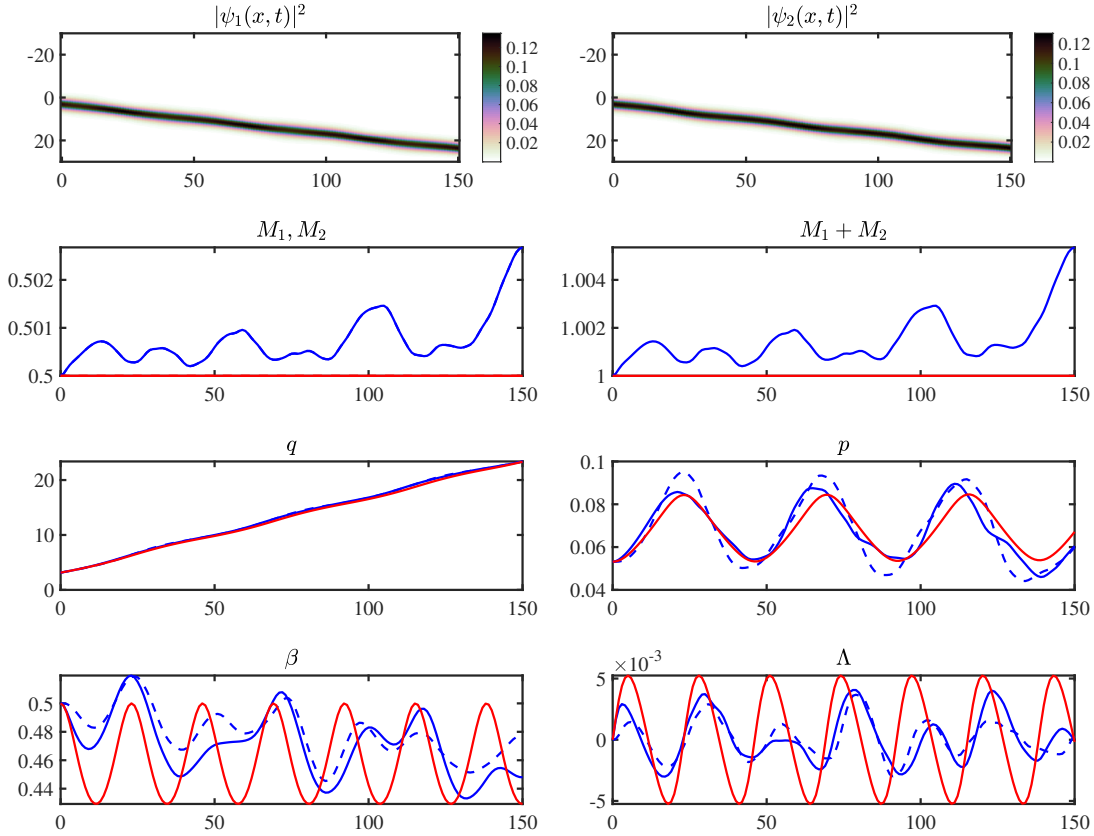


Figure 4. (Color online) Same as Fig. 2 but for the case 3 of Table 1. Again, the top left and right panels demonstrate the spatio-temporal evolution of the densities $|\psi_1|^2$ and $|\psi_2|^2$, respectively. The blue lines in the second, third, and fourth rows correspond to numerical results of the Schrödinger's equation whereas the red lines to the 8CC variational calculation. Finally, the solid and dashed lines correspond to the first and second component, respectively.

that in case 4, with $M_1 + M_2$ as well as $\beta(t)$ slowly increasing, which eventually leads to blowup. This instability is seen in the $p(v)$ curve shown in 7.

8. Dynamical stability using the stability curve $p(v)$

In references [22, 26, 27] it was shown that the stability of a solitary wave subjected to external forces could be inferred from the solution of the CC equations by studying the stability curve $p(v)$, where $p(t)$ is the momentum conjugate to $q(t)$ and $v(t) \equiv \dot{q}(t)$. A positive slope of the p vs v curve is a necessary condition for the stability of the solitary wave. If a branch of the $p(v)$ curve has a negative slope, this is a sufficient condition for instability. In our simulations, we will show that this criterion is consistent with the numerical simulations, (see Fig. 7). Note that in the present setup, exact solutions are no longer available once we add the external potential, and simultaneously, the CC equations do not possess exact solutions of the form $q(t) = q_0 + v_s t$, $\beta(t) = \beta_0$, $p(t) = p_0$, and $\theta_i(t) = \theta_{0,i} + \gamma_i t$. Because of this, we cannot perform a phase portrait analysis for

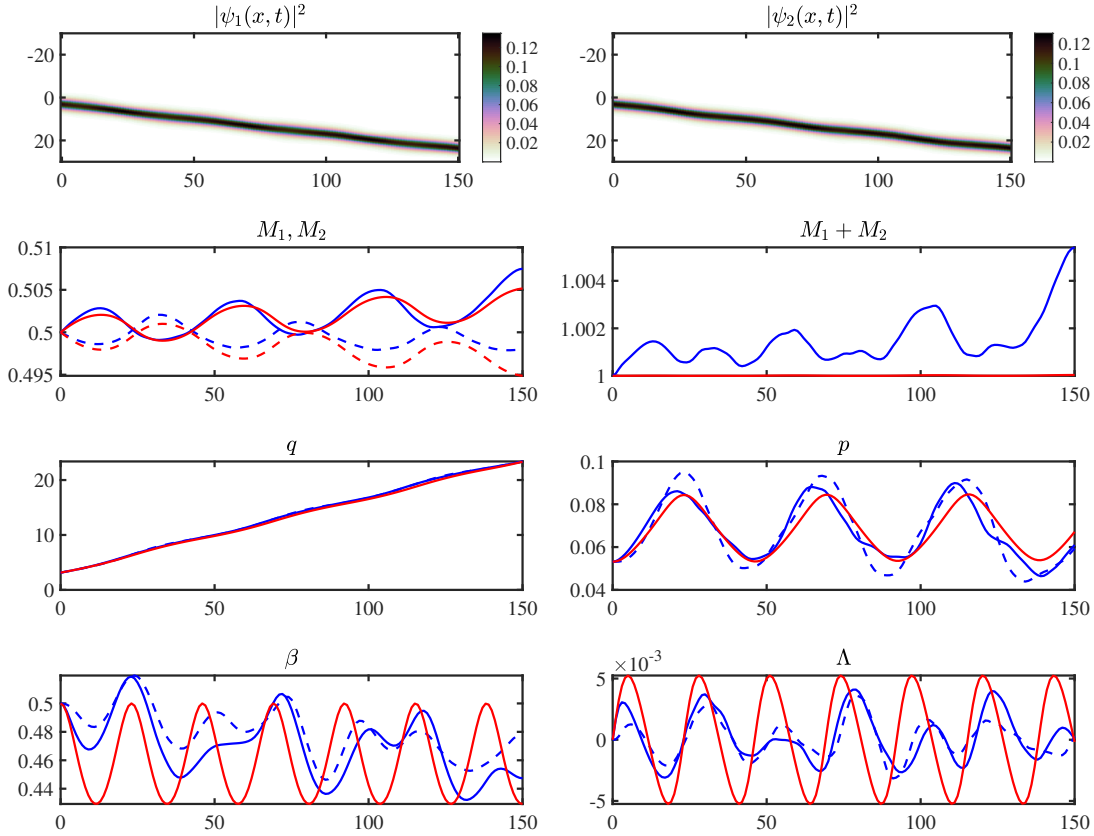


Figure 5. (Color online) Same as Fig. 2 but for the case 4 of Table 1. The top left and right panels demonstrate the spatio-temporal evolution of the densities $|\psi_1|^2$ and $|\psi_2|^2$, respectively. The blue lines in the second, third, and fourth rows correspond to numerical results of the Schrödinger's equation whereas the red lines to the 8CC variational calculation. Again, the solid and dashed lines correspond to the first and second component, respectively.

solutions which are near these fixed-point solutions of the CC equations. Nevertheless, for most of the cases where instabilities occur, $p(v)$ is a good indicator of instability. Indeed, we show four cases where this turnaround is clearly visible both for the trapped as well as moving soliton. It is only when $a_2 = 0$ (case 3) that we did not detect a place where $dp/dv < 0$ in our CC evolutions. When we increase the value of $|a_2|$ to be greater than $1/300$ the turnaround of the curve is much more visible than at $a_2 = -1/1000$. We have included the numerically determined curves $p_i(v_i)$ which show this turnaround more dramatically at $a_2 = -1/1000$.

9. Conclusions

To understand the difference between the effect of \mathcal{PT} -symmetric vs \mathcal{PT} -antisymmetric external potentials on solitary wave dynamics, the present work generalized the \mathcal{PT} symmetric external potential problem studied in [21], to a two-component NLSE in a \mathcal{PT} -antisymmetric external potential. Imposing anti- \mathcal{PT} symmetry on the exact

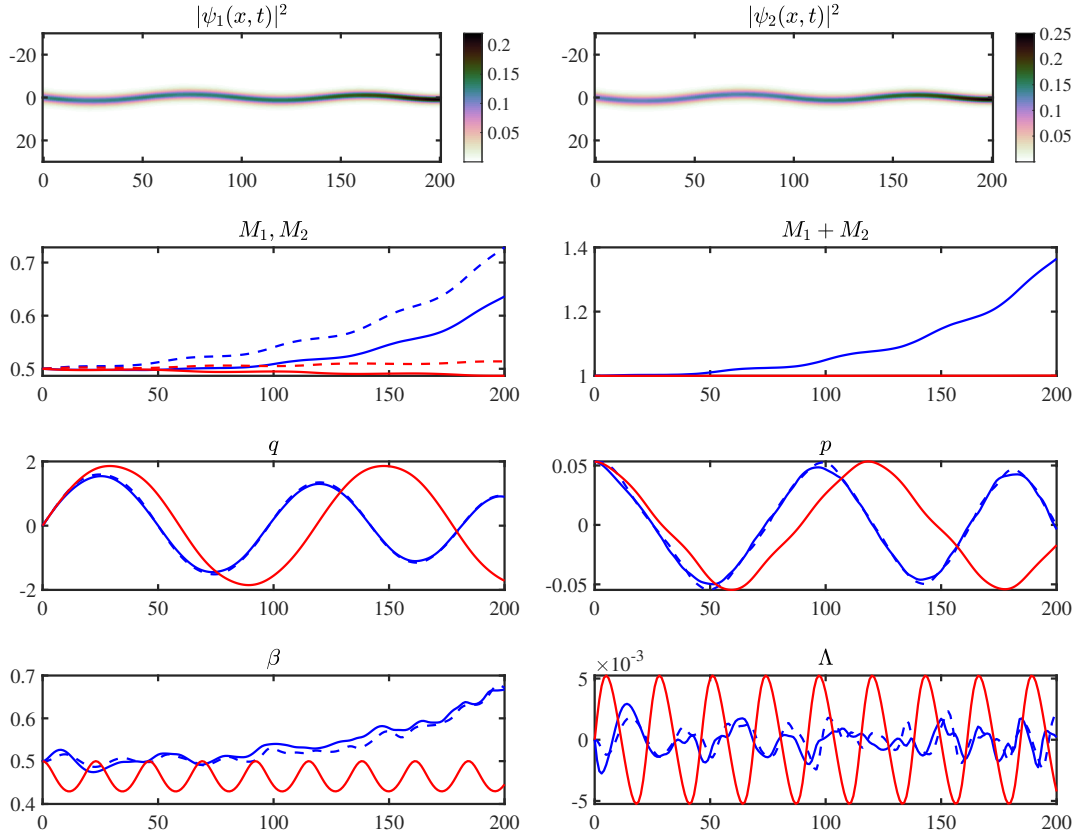


Figure 6. (Color online) Same as Fig. 2 but for the case 5 of Table 1. All panels have the same format as the ones of Figs. 3-5.

solution in the absence of the external potential requires that the masses of the two components are equal, and that the phases differ by $\pi/2$. Depending on initial conditions, the real external periodic potential can trap the solitary wave. On the other hand, the two imaginary anti- \mathcal{PT} external potentials affect the solitary wave differently. In particular, the potential term proportional to σ_3 causes M_1 and M_2 to initially move in opposite directions. Which way the masses diverge depends on the sign of $a_2 \cos k_2 q(0)$. The term in the potential proportional to a_3 becomes more important when the term proportional to σ_3 causes M_1 to differ from M_2 . Then it tends to accelerate the collapse of one component and/or accelerate the blowup or collapse of the entire soliton. Otherwise, when $a_2 = 0$, the effect of a_3 on the behavior of the soliton is initially quite small and is negligible in the CC approximation. However, the numerical simulations show that eventually the presence of a_3 leads to an instability. When $a_2 \geq 1/1000$, we observe that the instability criterion determined by $dp/dv \leq 0$ is being met, and can be seen visually either in the 8CC approximation or the numerical solution of the moment equations. We displayed cases where $M_1 + M_2$ and $\beta(t)$ get larger and larger signaling blowup. Even in the trapped cases, when a_2 is still quite small, the $p(v)$ criterion predicts dynamic instability which is seen in the simulations.

In all cases the lower order moments, $M_1(t)$, $M_2(t)$, $q(t)$, and $p(t)$ are well described

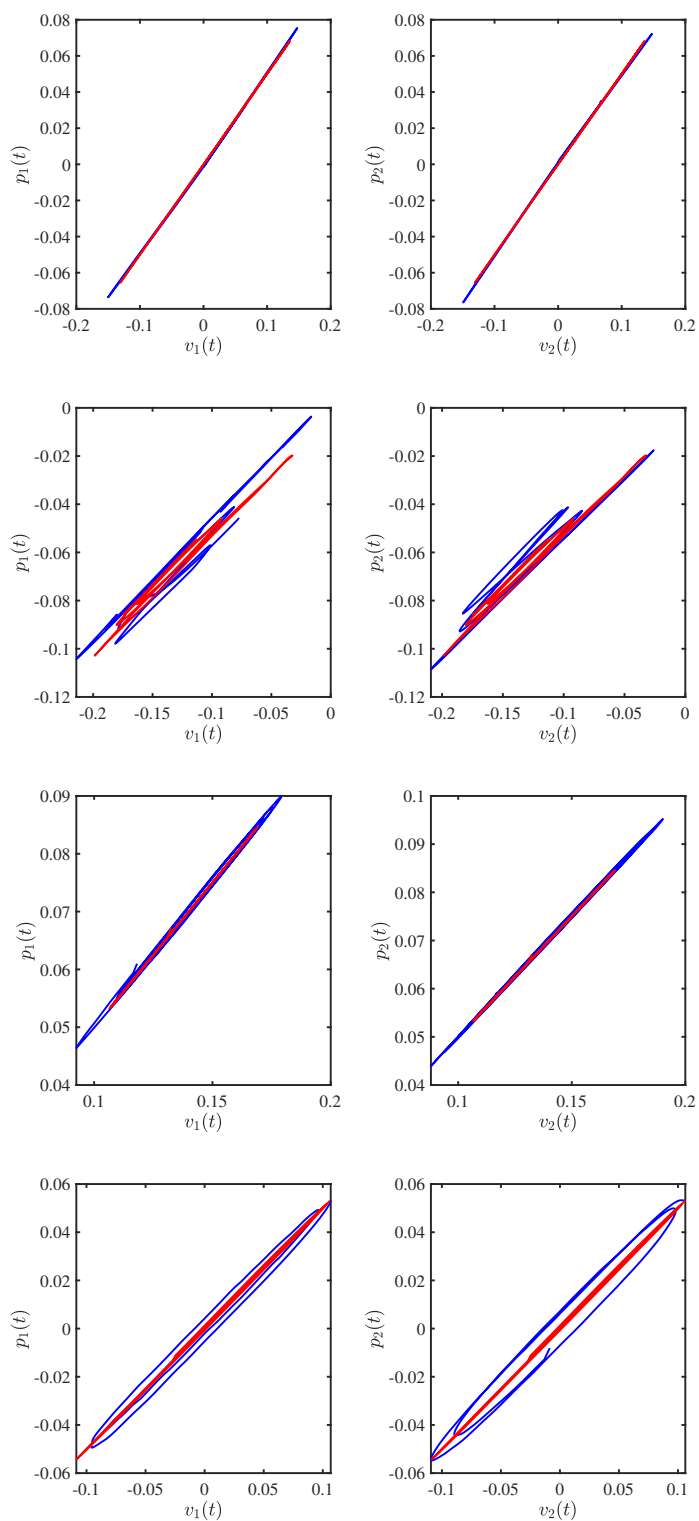


Figure 7. Plots of $p(v)$. Case 1 (top row), Case 2 (second row), Case 4 (third row), and Case 5 (fourth row). In many cases, the change of slope is not visible. The red lines are the 8CC results whereas the blue lines are the PDE results. Even though the 8CC (red) curves look linear in some cases, in fact (under detailed examination) they are not and indicate instability.

by the CC equations whereas $\beta(t)$ and $\Lambda(t)$ are just qualitatively in agreement with the numerical solution of the PDEs. The values $g = 2$ and $\beta(0) = 1/2$ were chosen to compare our results with the \mathcal{PT} -symmetric single-component NLSE results. Because of the destabilizing effect of σ_2 , there is in general no small oscillation theory for the anti- \mathcal{PT} external potential problem. This is a major difference from the \mathcal{PT} -symmetric one-component NLSE. Whenever $a_2 \neq 0$ holds, one finds dynamic instability which explains why we were unable to find stable solutions of the anti- \mathcal{PT} symmetric NLSE in the presence of an anti- \mathcal{PT} symmetric external potential. We considered cases in this paper where the soliton was trapped by the real potential $V_0(x)$ as well as cases where the solitary wave was moving. In both cases the 8CC approximation gave a reasonable description of the motion of the two components of the wave function. The phase space of possible behaviors is huge, and we reported on a few representative cases.

This work paves the way for future directions of study. At the level of the NLSEs, a systematic stability analysis around the steady-state and moving soliton solutions over (a_1, a_2, a_3) will identify potential intervals of stability of the pertinent waveforms. If the solutions obtained are identified as unstable, then it would be interesting to corroborate even further our dynamical instability criterion employed in this work, i.e., $dp/dv < 0$. Also, another direction of future work involves other kind of external potentials, such as hyperbolic ones in the form of $V_1(x) = \text{sech } x \tanh x$ and $V_2(x) = iW(x) = i \text{sech}^2 x$. Those directions are currently under consideration and results will be reported in future publications.

Acknowledgments

EGC, FC and JFD would like to thank the Santa Fe Institute and the Center for Nonlinear Studies at Los Alamos National Laboratory for their hospitality. AK is grateful to Indian National Science Academy (INSA) for awarding him INSA Senior Scientist position at Savitribai Phule Pune University, Pune, India. The work of AS was supported by the U.S. Department of Energy.

Appendix A. Derivation of the eight component CC equations of motion

Appendix A.1. Dynamic term

From Eq.(4.4), the dynamic term splits into the sum of two independent parts:

$$T(Q, \dot{Q}) = t_1(Q, \dot{Q}) + t_2(Q, \dot{Q}) = \pi_\mu(Q) \dot{Q}^\mu, \quad (\text{A.1})$$

where

$$t_1(Q, \dot{Q}) = M_1 \left\{ \dot{\theta}_1 + p \dot{q} - \frac{\pi^2}{12\beta^2} \dot{\Lambda} \right\}, \quad (\text{A.2a})$$

$$t_2(Q, \dot{Q}) = M_2 \left\{ \dot{\theta}_2 + p \dot{q} - \frac{\pi^2}{12\beta^2} \dot{\Lambda} \right\}, \quad (\text{A.2b})$$

so that

$$\pi_{\theta_1} = M_1, \quad \pi_{\theta_2} = M_2, \quad \pi_q = (M_1 + M_2)p, \quad \pi_\Lambda = -\frac{\pi^2}{12\beta^2}(M_1 + M_2). \quad (\text{A.3})$$

From these expressions, the symplectic matrix is:

$$f_{\mu\nu}(Q) = \partial_\mu \pi_\nu - \partial_\nu \pi_\mu = \begin{pmatrix} 0 & 1 & 0 & 0 & p & 0 & 0 & -c \\ -1 & 0 & 0 & 0 & 0 & 0 & 0 & 0 \\ 0 & 0 & 0 & 1 & p & 0 & 0 & -c \\ 0 & 0 & -1 & 0 & 0 & 0 & 0 & 0 \\ -p & 0 & -p & 0 & 0 & -M & 0 & 0 \\ 0 & 0 & 0 & 0 & M & 0 & 0 & 0 \\ 0 & 0 & 0 & 0 & 0 & 0 & 0 & Md \\ c & 0 & c & 0 & 0 & 0 & -Md & 0 \end{pmatrix}, \quad (\text{A.4})$$

where

$$M = M_1 + M_2, \quad c = \frac{\pi^2}{12\beta^2}, \quad d = \frac{\pi^2}{6\beta^3}. \quad (\text{A.5})$$

The determinant of $f_{\mu\nu}(Q)$ is $d^2 M^4$, and its inverse is given by:

$$f^{\mu\nu}(Q) = \frac{1}{M} \begin{pmatrix} 0 & -M & 0 & 0 & 0 & 0 & 0 & 0 \\ M & 0 & 0 & 0 & 0 & -p & c/d & 0 \\ 0 & 0 & 0 & -M & 0 & 0 & 0 & 0 \\ 0 & 0 & M & 0 & 0 & -p & c/d & 0 \\ 0 & 0 & 0 & 0 & 0 & 1 & 0 & 0 \\ 0 & p & 0 & p & -1 & 0 & 0 & 0 \\ 0 & -c/d & 0 & -c/d & 0 & 0 & 0 & -1/d \\ 0 & 0 & 0 & 0 & 0 & 0 & 1/d & 0 \end{pmatrix}, \quad (\text{A.6})$$

where

$$\frac{1}{d} = \frac{6\beta^3}{\pi^2}, \quad \frac{c}{d} = \frac{\beta}{2}. \quad (\text{A.7})$$

Appendix A.2. Hamiltonian and its decomposition

Based on Eq. (4.6), the Hamiltonian can be written as the sum of three parts:

$$H(Q) = H_{\text{kin}}(Q) + H_{\text{pot}}(Q) + H_{\text{nl}}(Q), \quad (\text{A.8})$$

where H_{kin} , H_{pot} , H_{nl} stand for the kinetic, potential, and nonlinear terms, respectively.

Let us consider the kinetic term first. Using the integral definitions of Appendix B, we find:

$$H_{\text{kin}}(Q) = \int dx |\partial_x \Psi_i(x, Q)|^2 = M \left\{ p^2 + \frac{1}{3} \beta^2 + \frac{\pi^2}{3} \frac{\Lambda^2}{\beta^2} \right\}. \quad (\text{A.9})$$

In a similar fashion, the potential term gives

$$\begin{aligned} H_{\text{pot}}(Q) &= \int dx V_0(x) |\Psi(x, t)|^2 = [A_1^2 \beta + A_2^2 \beta] \beta a_1 \int dx \operatorname{sech}^2[\beta(x - q)] \cos k_1 x \\ &= \frac{M}{2} a_1 \cos(k_1 q) G_1(k_1/\beta), \end{aligned} \quad (\text{A.10})$$

where $G_1(z)$ is given in (B.1a). Finally, we consider the nonlinear term,

$$H_{\text{nl}}(Q) = -\frac{g}{2} \int dx |\Psi(x, Q)|^4 = -\frac{g}{6} \beta M^2. \quad (\text{A.11})$$

From (A.9), (A.10), and (A.11), the Hamiltonian is given by

$$H(Q) = M \left\{ p^2 + \frac{1}{3} \beta^2 + \frac{\pi^2}{3} \frac{\Lambda^2}{\beta^2} + \frac{a_1}{2} \cos(k_1 q) G_1(k_1/\beta) \right\} - \frac{g}{6} \beta M^2. \quad (\text{A.12})$$

Defining

$$v_\mu(Q) = \partial_\mu H(Q), \quad (\text{A.13})$$

the nonzero derivatives of the Hamiltonian with respect to the parameters are given by:

$$v_{M_1} = v_{M_2} = p^2 + \frac{1}{3} \beta^2 + \frac{\pi^2}{3} \frac{\Lambda^2}{\beta^2} + \frac{a_1}{2} \cos(k_1 q) G_1(k_1/\beta) - \frac{g}{3} \beta M, \quad (\text{A.14a})$$

$$v_q = -M \frac{k_1 a_1}{2} \sin(k_1 q) G_1(k_1/\beta), \quad (\text{A.14b})$$

$$v_p = 2 M p, \quad (\text{A.14c})$$

$$v_\beta = M \left\{ \frac{2}{3} \beta - \frac{2\pi^2}{3} \frac{\Lambda^2}{\beta^3} - \frac{a_1 k_1}{2\beta^2} \cos(k_1 q) G'_1(k_1/\beta) \right\} - \frac{g}{6} M^2, \quad (\text{A.14d})$$

$$v_\Lambda = M \frac{2\pi^2}{3} \frac{\Lambda}{\beta^2}. \quad (\text{A.14e})$$

Here $G'_1(z)$ is given in (B.1d).

Appendix A.3. Dissipative term

From (2.11) and (4.7), the dissipative term splits into two parts. We find

$$\begin{aligned} F(Q, \dot{Q}) &= i \int dx \{ \Psi^\dagger(x, Q) U_1(x) \Psi_t(x, Q) - \Psi_t^\dagger(x, Q) U_1(x) \Psi(x, Q) \} \\ &= F_1(Q, \dot{Q}) + F_2(Q, \dot{Q}), \end{aligned} \quad (\text{A.15})$$

where

$$F_1(Q, \dot{Q}) = a_2 [F_{11}(Q, \dot{Q}) - F_{22}(Q, \dot{Q})], \quad (\text{A.16a})$$

$$F_2(Q, \dot{Q}) = a_3 [F_{12}(Q, \dot{Q}) + F_{21}(Q, \dot{Q})], \quad (\text{A.16b})$$

with

$$F_{ii}(Q, \dot{Q}) = -2 \int dx \cos(k_2 x) \text{Im} \{ \psi_i^*(x, Q) \partial_t \psi_i(x, Q) \}, \quad (\text{A.17a})$$

$$F_{12}(Q, \dot{Q}) = -2 \int dx \cos(k_3 x) \text{Im} \{ \psi_1^*(x, Q) \partial_t \psi_2(x, Q) \}, \quad (\text{A.17b})$$

$$F_{21}(Q, \dot{Q}) = -2 \int dx \cos(k_3 x) \text{Im} \{ \psi_2^*(x, Q) \partial_t \psi_1(x, Q) \}. \quad (\text{A.17c})$$

Changing variables to $y = \beta(x - q)$, we find

$$\begin{aligned}
F_{ii}(Q, \dot{Q}) &= M_i \int dy \cos \left[k_2 \left(\frac{y}{\beta} + q \right) \right] \left\{ \dot{\theta}_i - \frac{\dot{p}}{\beta} y + p \dot{q} - \frac{\dot{\Lambda}}{\beta^2} y^2 + \frac{2\Lambda \dot{q}}{\beta} y \right\} \operatorname{sech}^2(y) \\
&= M_i \{ \cos(k_2 q) [(\dot{\theta}_i + p \dot{q}) G_1(k_2/\beta) - (\dot{\Lambda}/\beta^2) G_2(k_2/\beta)] \\
&\quad + \sin(k_2 q) [(\dot{p} - 2\Lambda \dot{q})/\beta] G_3(k_2/\beta) \}.
\end{aligned} \tag{A.18}$$

So from (A.16a), we find

$$\begin{aligned}
F_1(Q, \dot{Q}) &= a_2 M_1 \{ \cos(k_2 q) [(\dot{\theta}_1 + p \dot{q}) G_1(k_2/\beta) - (\dot{\Lambda}/\beta^2) G_2(k_2/\beta)] \\
&\quad + \sin(k_2 q) [(\dot{p} - 2\Lambda \dot{q})/\beta] G_3(k_2/\beta) \} \\
&\quad - a_2 M_2 \{ \cos(k_2 q) [(\dot{\theta}_2 + p \dot{q}) G_1(k_2/\beta) - (\dot{\Lambda}/\beta^2) G_2(k_2/\beta)] \\
&\quad + \sin(k_2 q) [(\dot{p} - 2\Lambda \dot{q})/\beta] G_3(k_2/\beta) \}.
\end{aligned} \tag{A.19}$$

Defining

$$w_{1,\mu}(Q) = \frac{\partial F_1(Q, \dot{Q})}{\partial \dot{Q}^\mu}, \tag{A.20}$$

we find the non-zero components are:

$$w_{1,\theta_1} = a_2 M_1 \cos(k_2 q) G_1(k_2/\beta), \tag{A.21a}$$

$$w_{1,\theta_2} = -a_2 M_2 \cos(k_2 q) G_1(k_2/\beta), \tag{A.21b}$$

$$w_{1,q} = a_2 (M_1 - M_2) \left[p \cos(k_2 q) G_1(k_2/\beta) - \frac{2\Lambda}{\beta} \sin(k_2 q) G_3(k_2/\beta) \right], \tag{A.21c}$$

$$w_{1,p} = a_2 \frac{M_1 - M_2}{\beta} \sin(k_2 q) G_3(k_2/\beta), \tag{A.21d}$$

$$w_{1,\Lambda} = -a_2 \frac{M_1 - M_2}{\beta^2} \cos(k_2 q) G_2(k_2/\beta). \tag{A.21e}$$

For $F_{12}(Q, \dot{Q})$ and again setting $y = \beta(x - q)$, we find

$$\begin{aligned}
F_{12}(Q, \dot{Q}) &= -2 \int dx \cos(k_3 x) \operatorname{Im} \{ \psi_1^*(x, t) [\partial_t \psi_2(x, t)] \} \\
&= \sqrt{M_1 M_2} \int dy \cos[k_3 (y/\beta) + k_3 q] \operatorname{sech}^2(y) \\
&\quad \times \{ \cos(\theta_1 - \theta_2) [-\dot{p} y/\beta + p \dot{q} - \dot{\Lambda} y^2/\beta^2 + 2\Lambda \dot{q} y/\beta + \dot{\theta}_2] \\
&\quad - \sin(\theta_1 - \theta_2) [\dot{A}_2/A_2 + \dot{\beta}/\beta - (\dot{\beta} y/\beta - \beta \dot{q}) \tanh(y)] \}.
\end{aligned} \tag{A.22}$$

Simplifying, we obtain

$$\begin{aligned}
F_{12}(Q, \dot{Q}) &= \sqrt{M_1 M_2} \\
&\times \{ \cos(k_3 q) \cos(\theta_1 - \theta_2) [(\dot{\theta}_2 + p \dot{q}) G_1(z) - (\dot{\Lambda}/\beta^2) G_2(z)] \\
&\quad - \cos(k_3 q) \sin(\theta_1 - \theta_2) [\dot{M}_2/M_2 + \dot{\beta}/\beta] G_1(z)/2 + (\dot{\beta}/\beta) G_5(z)] \\
&\quad + \sin(k_3 q) \cos(\theta_1 - \theta_2) [(\dot{p} - 2\Lambda \dot{q}) G_3(z)/\beta] \\
&\quad + \sin(k_3 q) \sin(\theta_1 - \theta_2) [\beta \dot{q} G_4(z)] \}.
\end{aligned} \tag{A.23}$$

Similarly,

$$\begin{aligned}
F_{21}(Q, \dot{Q}) &= \sqrt{M_1 M_2} \\
&\times \{ \cos(k_3 q) \cos(\theta_1 - \theta_2) [(\dot{\theta}_1 + p \dot{q}) G_1(z) - (\dot{\Lambda}/\beta^2) G_2(z)] \\
&\quad + \cos(k_3 q) \sin(\theta_1 - \theta_2) [\dot{M}_1/M_1 + \dot{\beta}/\beta] G_1(z)/2 + (\dot{\beta}/\beta) G_5(z)] \\
&\quad + \sin(k_3 q) \cos(\theta_1 - \theta_2) [(\dot{p} - 2\Lambda \dot{q}) G_3(z)/\beta] \\
&\quad - \sin(k_3 q) \sin(\theta_1 - \theta_2) [\beta \dot{q} G_4(z)] \}.
\end{aligned} \tag{A.24}$$

So from (A.16b), combining (A.23) and (A.24), we get

$$\begin{aligned}
F_2(Q, \dot{Q}) &= a_3 [F_{12}(Q, \dot{Q}) + F_{21}(Q, \dot{Q})] \\
&= a_3 \sqrt{M_1 M_2} \\
&\times \{ \cos(k_3 q) \cos(\theta_1 - \theta_2) [(\dot{\theta}_1 + \dot{\theta}_2 + 2p \dot{q}) G_1(z) - 2(\dot{\Lambda}/\beta^2) G_2(z)] \\
&\quad + \cos(k_3 q) \sin(\theta_1 - \theta_2) [(\dot{M}_1/M_1 - \dot{M}_2/M_2) G_1(z)/2] \\
&\quad + \sin(k_3 q) \cos(\theta_1 - \theta_2) [2(\dot{p} - 2\Lambda \dot{q}) G_3(z)/\beta] \}.
\end{aligned} \tag{A.25}$$

Defining

$$w_{2,\mu}(Q) = \frac{\partial F_2(Q, \dot{Q})}{\partial \dot{Q}^\mu}, \tag{A.26}$$

we find

$$w_{2,M_1} = a_3 \sqrt{M_2/M_1} \cos(k_3 q) \sin(\theta_1 - \theta_2) G_1(k_3/\beta)/2, \tag{A.27a}$$

$$w_{2,\theta_1} = a_3 \sqrt{M_1 M_2} \cos(k_3 q) \cos(\theta_1 - \theta_2) G_1(k_3/\beta), \tag{A.27b}$$

$$w_{2,M_2} = -a_3 \sqrt{M_1/M_2} \cos(k_3 q) \sin(\theta_1 - \theta_2) G_1(k_3/\beta)/2, \tag{A.27c}$$

$$w_{2,\theta_2} = a_3 \sqrt{M_1 M_2} \cos(k_3 q) \cos(\theta_1 - \theta_2) G_1(k_3/\beta), \tag{A.27d}$$

$$\begin{aligned}
w_{2,q} &= a_3 \sqrt{M_1 M_2} \{ \cos(k_3 q) \cos(\theta_1 - \theta_2) 2p G_1(k_3/\beta) \\
&\quad - \sin(k_3 q) \cos(\theta_1 - \theta_2) (4\Lambda/\beta) G_3(k_3/\beta) \},
\end{aligned} \tag{A.27e}$$

$$w_{2,p} = a_3 \sqrt{M_1 M_2} \sin(k_3 q) \cos(\theta_1 - \theta_2) (2/\beta) G_3(k_3/\beta), \tag{A.27f}$$

$$w_{2,\beta} = 0, \tag{A.27g}$$

$$w_{2,\Lambda} = -a_3 \sqrt{M_1 M_2} \cos(k_3 q) \cos(\theta_1 - \theta_2) (2/\beta^2) G_2(k_3/\beta). \tag{A.27h}$$

Appendix A.4. Equations of motion

From (4.13), the equations of motion are found from

$$\dot{Q}^\mu = f^{\mu\nu}(Q) u_\nu(Q), \quad u_\mu(Q) = v_\mu(Q) - w_\mu(Q). \tag{A.28}$$

Let us first find $u_\mu(Q)$. From (A.14a), (A.21a), and (A.27a),

$$\begin{aligned}
u_{M_1} &= p^2 + \frac{1}{3} \beta^2 + \frac{\pi^2}{3} \frac{\Lambda^2}{\beta^2} + \frac{a_1}{2} \cos(k_1 q) G_1(k_1/\beta) - \frac{g}{3} \beta M \\
&\quad - a_3 \sqrt{M_2/M_1} \cos(k_3 q) \sin(\theta_1 - \theta_2) G_1(k_3/\beta)/2,
\end{aligned} \tag{A.29a}$$

$$\begin{aligned}
u_{\theta_1} &= -a_2 M_1 \cos(k_2 q) G_1(k_2/\beta) \\
&\quad - a_3 \sqrt{M_1 M_2} \cos(k_3 q) \cos(\theta_1 - \theta_2) G_1(k_3/\beta),
\end{aligned} \tag{A.29b}$$

$$u_{M_2} = p^2 + \frac{1}{3} \beta^2 + \frac{\pi^2}{3} \frac{\Lambda^2}{\beta^2} + \frac{a_1}{2} \cos(k_1 q) G_1(k_1/\beta) - \frac{g}{3} \beta M \quad (\text{A.29c})$$

$$+ a_3 \sqrt{M_1/M_2} \cos(k_3 q) \sin(\theta_1 - \theta_2) G_1(k_3/\beta)/2 ,$$

$$u_{\theta_2} = a_2 M_2 \cos(k_2 q) G_1(k_2/\beta) - a_3 \sqrt{M_1 M_2} \cos(k_3 q) \cos(\theta_1 - \theta_2) G_1(k_3/\beta) , \quad (\text{A.29d})$$

$$u_q = -M \frac{k_1 a_1}{2} \sin(k_1 q) G_1(k_1/\beta) - a_2 (M_1 - M_2) [p \cos(k_2 q) G_1(k_2/\beta) - (2\Lambda/\beta) \sin(k_2 q) G_3(k_2/\beta)] - a_3 \sqrt{M_1 M_2} \{ \cos(k_3 q) \cos(\theta_1 - \theta_2) 2p G_1(k_3/\beta) - \sin(k_3 q) \cos(\theta_1 - \theta_2) (4\Lambda/\beta) G_3(k_3/\beta) \} , \quad (\text{A.29e})$$

$$u_p = M 2p - a_2 \frac{M_1 - M_2}{\beta} \sin(k_2 q) G_3(k_2/\beta) - a_3 \sqrt{M_1 M_2} \sin(k_3 q) \cos(\theta_1 - \theta_2) (2/\beta) G_3(k_3/\beta) , \quad (\text{A.29f})$$

$$u_\beta = M \left\{ \frac{2}{3} \beta - \frac{2\pi^2}{3} \frac{\Lambda^2}{\beta^3} - \frac{a_1 k_1}{2\beta^2} \cos(k_1 q) G'_1(k_1/\beta) \right\} - \frac{g}{6} M^2 , \quad (\text{A.29g})$$

$$u_\Lambda = M \frac{2\pi^2}{3} \frac{\Lambda}{\beta^2} + a_2 \frac{M_1 - M_2}{\beta^2} \cos(k_2 q) G_2(k_2/\beta) + a_3 \sqrt{M_1 M_2} \cos(k_3 q) \cos(\theta_1 - \theta_2) (2/\beta^2) G_2(k_3/\beta) . \quad (\text{A.29h})$$

Using (A.6) and (A.29a) and (4.13), we obtain the 8CC equations of motion as given by Eqs. (5.8a).

Appendix B. Useful integrals and definitions

We define the following integrals:

$$G_1(z) := \int dy \cos(zy) \operatorname{sech}^2(y) = \pi z \operatorname{csch}(\pi z/2) , \quad (\text{B.1a})$$

$$G_2(z) := \int dy y^2 \cos(zy) \operatorname{sech}^2(y) = -\frac{\pi^2}{8} \operatorname{csch}^3(\pi z/2) [\pi z (3 + \cosh(\pi z)) - 4 \sinh(\pi z)] , \quad (\text{B.1b})$$

$$G_3(z) := \int dy y \sin(zy) \operatorname{sech}^2(y) = \frac{\pi}{2} \operatorname{csch}(\pi z/2) [-2 + \pi z \coth(\pi z/2)] , \quad (\text{B.1c})$$

$$G_4(z) := \int dy \sin(zy) \operatorname{sech}^2(y) \tanh(y) = \frac{\pi z^2}{2} \operatorname{csch}(\pi z/2) , \quad (\text{B.1d})$$

$$G_5(z) := \int dy y \cos(zy) \operatorname{sech}^2(y) \tanh(y) = \frac{\pi z}{4} [4 - \pi z \coth(\pi z/2)] \operatorname{csch}(\pi z/2) , \quad (\text{B.1e})$$

$$G_1'(z) = \pi \operatorname{csch}(\pi z/2) [1 - (\pi z/2) \coth(\pi z/2)]. \quad (\text{B.1f})$$

We note that

$$\frac{d}{dz} \operatorname{sech}(z) = -\operatorname{sech}(z) \tanh(z), \quad (\text{B.2a})$$

$$\frac{d}{dz} \tanh(z) = \operatorname{sech}^2(z), \quad (\text{B.2b})$$

together with the following useful integrals:

$$\int dz \operatorname{sech}^2(z) = 2, \quad (\text{B.3a})$$

$$\int dz \operatorname{sech}^4(z) = \frac{4}{3}, \quad (\text{B.3b})$$

$$\int dz z^2 \operatorname{sech}^2(z) = \frac{\pi^2}{6}. \quad (\text{B.3c})$$

Bibliography

- [1] C. M. Bender, *PT Symmetry in Classical and Quantum Physics* (World Scientific, London, 2019).
- [2] C. M. Bender and S. Boettcher, “Real spectra in non-Hermitian Hamiltonians having \mathcal{PT} symmetry,” *Phys. Rev. Lett.* **80**, 5243 (1998).
- [3] L. Ge and H. E. Türeci, “Antisymmetric \mathcal{PT} -photonic structures with balanced positive- and negative-index materials,” *Phys. Rev. A* **88**, 053810 (2013).
- [4] P. Peng, W. Cao, C. Shen, W. Qu, J. Wen, L. Jiang, and Y. Xiao, “Anti-parity, anti-time symmetry with flying atoms,” *Nat. Phys.* **12**, 1139 (2016).
- [5] X.-L. Zhang, T. Jiang, and C. T. Chan, “Dynamically encircling an exceptional point in anti-parity-time symmetric systems: Asymmetric mode switching for symmetry broken modes,” *Light Sci. Appl.* **8**, 1 (2019).
- [6] Y. Choi, C. Hahn, J.W. Yoon, and S. H. Song, “Observation of an anti- \mathcal{PT} -symmetric exceptional point and energy difference conserving dynamics in electrical circuit resonators,” *Nat. Commun.* **9**, 2182 (2018).
- [7] Y. Jiang, Y. Mei, Y. Zuo, Y. Zhai, J. Li, J. Wen, and S. Du, “Anti-parity-time symmetric optical four-wave mixing in cold atoms,” *Phys. Rev. Lett.* **123**, 193604 (2019).
- [8] F. Yang, Y.-C. Liu, and L. You, “Anti- \mathcal{PT} symmetry in dissipatively coupled optical systems,” *Phys. Rev. A* **96**, 053845 (2017).
- [9] X. Wang et al., “Optical \mathcal{PT} -symmetry and \mathcal{PT} -antisymmetry in coherently driven atomic lattices,” *Opt. Express* **24**, 4289 (2016).
- [10] Y.-L. Chuang et al., “Realization of simultaneously parity-time-symmetric and parity-time-antisymmetric susceptibilities along the longitudinal direction in atomic systems with all optical controls,” *Opt. Express* **26**, 21969 (2018).
- [11] V. V. Konotop and D. A. Zezyulin, “Odd-time reversal \mathcal{PT} -symmetry induced by an anti- \mathcal{PT} -symmetric medium,” *Phys. Rev. Lett.* **120**, 123902 (2018).
- [12] Q. Li et al., “Experimental simulation of anti-parity-time symmetric Lorentz dynamics,” *Optica* **6**, 67 (2019).
- [13] S. Ke et al. “Topological bound modes in anti- \mathcal{PT} -symmetric optical waveguide arrays,” *Opt. Express* **27**, 13858 (2019).
- [14] R. Couvreur, J. L. Jacobsen, and H. Saleur, “Entanglement in nonunitary quantum critical spin chains,” *Phys. Rev. Lett.* **119**, 040601 (2017).
- [15] T. E. Lee, F. Reiter, and N. Moiseyev, “Entanglement and spin squeezing in nonhermitian phase transitions,” *Phys. Rev. Lett.* **113**, 250401 (2014).
- [16] Y. Li et al., “Anti-parity-time symmetry in diffusive systems,” *Science* **364**, 170 (2019).

- [17] S. Chakraborty and D. Chruscinski, “Information flow versus divisibility for qubit evolution,” *Phys. Rev. A* **99**, 042105 (2019).
- [18] S. Haseli et al. “Non-Markovianity through flow of information between a system and an environment,” *Phys. Rev. A* **90**, 052118 (2014).
- [19] V. V. Konotop and D. A. Zezyulin, “Spectral singularities of odd- \mathcal{PT} -symmetric potentials,” *Phys. Rev. A* **99**, 013823 (2019). URL <https://link.aps.org/doi/10.1103/PhysRevA.99.013823>.
- [20] E. G. Charalampidis, J. F. Dawson, F. Cooper, A. Khare, A. Saxena. “Stability and response of trapped solitary wave solutions of coupled nonlinear Schrödinger equations in an external, \mathcal{PT} - and supersymmetric potential,” *J. Phys. A: Math. Theor.* **53** (2020); arXiv:2004:08940. Preprint number: LA-UR-20-2280.
- [21] F. G. Mertens, F. Cooper, E. Arévalo, A. Khare, A. Saxena, and A. R. Bishop, “Variational approach to studying solitary waves in the nonlinear Schrödinger equation with complex potentials,” *Phys. Rev. E* **94**, 032213 (2016). URL <http://link.aps.org/doi/10.1103/PhysRevE.94.032213>.
- [22] F. G. Mertens, N. R. Quintero, I. V. Barashenkov, and A. R. Bishop, “Refined empirical stability criterion for nonlinear Schrödinger solitons under spatiotemporal forcing,” *Phys. Rev. E* **84**, 026614 (2011). URL <https://link.aps.org/doi/10.1103/PhysRevE.84.026614>.
- [23] G. H. Derrick, “Comments on Nonlinear Wave Equations as Models for Elementary Particles,” *Journal of Mathematical Physics* **5**, 1252 (1964). <http://dx.doi.org/10.1063/1.1704233>, URL <http://dx.doi.org/10.1063/1.1704233>.
- [24] F. Cooper, A. Khare, A. Comech, B. Mihaila, J. F. Dawson, and A. Saxena, “Stability of exact solutions of the nonlinear Schrödinger equation in an external potential having supersymmetry and parity-time symmetry,” *J. Phys. A: Math. Theor.* **50**, 015391 (2017).
- [25] F. Cooper, J. F. Dawson, F. G. Mertens, E. Arévalo, N. R. Quintero, B. Mihaila, A. Khare, and A. Saxena, “Response of exact solutions of the nonlinear Schrödinger equation to small perturbations in a class of complex external potentials having supersymmetry and parity-time symmetry,” *J. of Phys. A: Math. and Theor.* **50**, 485205 (2017). URL <http://stacks.iop.org/1751-8121/50/i=48/a=485205>.
- [26] F. G. Mertens, N. R. Quintero, and A. R. Bishop, “Nonlinear Schrödinger equation with spatiotemporal perturbations,” *Phys. Rev. E* **81**, 016608 (2010). URL <https://link.aps.org/doi/10.1103/PhysRevE.81.016608>.
- [27] N. R. Quintero, F. G. Mertens, and A. R. Bishop, “Generalized traveling-wave method, variational approach, and modified conserved quantities for the perturbed nonlinear Schrödinger equation,” *Phys. Rev. E* **82**, 016606 (2010). URL <http://link.aps.org/doi/10.1103/PhysRevE.82.016606>.
- [28] E. Hairer, S.P. Nørsett and G. Wanner, *Solving ordinary differential equations I* (Springer-Verlag, Berlin, 1993).